Taylor & Francis
Taylor & Francis Group

Journal of Biomolecular Structure and Dynamics

ISSN: (Print) (Online) Journal homepage: https://www.tandfonline.com/loi/tbsd20

Synthesis, molecular modelling, FT-IR, Raman and NMR characterization, molecular docking and ADMET study of new nickel(II) complex with an N_4-tetradentate thiosemicarbazone

Songül Eğlence-Bakır, Sefa Celik, Musa Şahin, Aysen E. Ozel, Sevim Akyuz & Bahri Ülküseven

To cite this article: Songül Eğlence-Bakır, Sefa Celik, Musa Şahin, Aysen E. Ozel, Sevim Akyuz & Bahri Ülküseven (2021) Synthesis, molecular modelling, FT-IR, Raman and NMR characterization, molecular docking and ADMET study of new nickel(II) complex with an N_4-tetradentate thiosemicarbazone, Journal of Biomolecular Structure and Dynamics, 39:12, 4212-4224, DOI: 10.1080/07391102.2020.1775128

To link to this article: https://doi.org/10.1080/07391102.2020.1775128

JOURNAL OF BIOMOLECULAR STRUCTURE AND DYNAMICS
2021, VOL. 39, NO. 12, 4212–4224
https://doi.org/10.1080/07391102.2020.1775128

Synthesis, molecular modelling, FT-IR, Raman and NMR characterization, molecular docking and ADMET study of new nickel(II) complex with an N_4-tetradentate thiosemicarbazone

Songül Eğlence-Bakır[a], Sefa Celik[b], Musa Şahin[a], Aysen E. Ozel[b], Sevim Akyuz[c] and Bahri Ülküseven[d]

[a]Department of Chemistry, Science Faculty, Istanbul University, Istanbul, Turkey; [b]Department of Physics, Science Faculty, Istanbul University, Istanbul, Turkey; [c]Department of Physics, Science and Letters Faculty, Istanbul Kultur University, Istanbul, Turkey; [d]Department of Chemistry, Engineering Faculty, Istanbul University-Cerrahpaşa, Istanbul, Turkey

Communicated by Ramaswamy H. Sarma

ABSTRACT

A new nickel(II) complex was synthesized by using *S*-propyl-thiosemicarbazide and 2-amino-3,5-dibromobenzaldehyde. The complex, obtained by the template effect of nickel ions, was structurally analysed by experimental and theoretical vibrational spectroscopy, NMR and density functional theory (DFT) calculations. By using DFT/B3LYP method with 6-311++G(d, p) basis set, the most stable molecular structure of the title molecule was calculated. The fundamental vibrational wavenumbers, IR and Raman intensities for the optimized structure of the molecule under investigation were determined and compared with the experimental vibrational spectra. The vibrational assignment was achieved using the calculated potential energy distributions of the vibrational modes. Moreover, the molecular electrostatic potential (MEP), the highest occupied molecular orbital (HOMO) and the lowest occupied molecular orbital (LUMO) energies were calculated, Molecular docking of the molecule was carried out against DNA in order to identify the potential inhibitory action of the title compound. The findings suggested that the aforementioned compound has a strong binding affinity to interact with DNA residues DT8, DC9, DG12, DG16, DA17, and DA18 through the intermolecular hydrogen bonds. Also the performed *in silico* ADMET analysis was the prediction of the synthesized molecule's pharmacokinetic and toxicity profile expressing good oral drug like actions and non-toxic nature. The complex has been shown to have the possibility to become a model molecule for drug development processes.

ARTICLE HISTORY
Received 29 March 2020
Accepted 22 May 2020

KEYWORDS
thiosemicarbarbazone; nickel(II) complex; DFT calculations; molecular docking; ADMET

1. Introduction

Thiosemicarbazone derivatives are an important class of Schiff base ligands obtained by condensation of thiosemicarbazide and carbonyl compounds (Leovac et al., 1982; Nehar et al., 2020). After the discovery of their activities on biological systems in 1950s, researchers have shown an increased interest in thiosemicarbazone compounds with nitrogen-rich conjugated structures (Behnisch et al., 1950; Matsa et al., 2019). Besides, thiosemicarabazones are used as versatile chelators for many metal ions due to their donor sets of hard nitrogen and soft sulphur atoms (Bisceglie et al., 2020; Güveli et al., 2016). Thiosemicarbazone molecules can bind to a metal centre in different coordination modes, and commonly bi- and tridentate ones use nitrogen, sulphur and/or oxygen from carbonyl moiety (Eglence-Bakir et al., 2019; Padhye & Kauffman, 1985; Sankaraperumal et al., 2013).

Tetradendate thiosemicarbazone ligands can be obtained by substitutions containing additional donor sites to both the azomethine and the amide group. In these studies, mostly 2-hydroxy aldehydes or ketones are used, resulting in the formation of metal complexes with N_2O_2 donor environment (Bal-Demirci et al., 2014; Kurt et al., 2013). It is shown that in recent years, the synthesis and characterization of donor ligands of nitrogen and sulphur has been one of the important research areas of coordination chemistry. Thiosemicarbazones (TSC) and their metal complexes have gained significant attention among the nitrogen/sulphur compounds due to their essential biological activities such as anti-cancer, anti-viral, anti-bacterial, anti-fungal, anti-tumor, anti-tuberculosis and anti-leprosia. Mostly they are used as anti-parasitic, antimalarial and anti-amoebial agents (Adams et al., 2013; Bautista et al., 2013; Casas et al., 2000; Ghogomu & Nkungli, 2016; Mishra et al., 2006; Netalkar et al., 2014, 2015). TSC's transition metal complexes are biologically more active than those of the free ligands. Not only does the presence of metal ions boost biological activity, chemical stability, but it also decreases side effects (Pelosi, 2010).

In our previous work, copper (II) and nickel (II) complexes, having asymmetric donor sets, ON_3 and N_3O, were synthesized by template condensation using a 2-amino-aldehyde in addition to a 2-hydroxy-aldehyde (Şahin et al., 2020). Here, we presented a new synthesis of nickel(II) complex with an

CONTACT Sefa Celik scelik@istanbul.edu.tr Department of Physics, Science Faculty, Istanbul University, Istanbul 34134, Turkey
Supplemental data for this article can be accessed online at https://doi.org/10.1080/07391102.2020.1775128.

N_4-chelating thiosemicarbazone ligand (Figure 1). Conformation properties and structural and vibrational characteristics of the complex were carried out by using experimental and theoretical methods. Moreover, to investigate its drug-receptor ability, NiL-DNA interaction was studied by molecular docking, and its toxicity, pharmacokinetic profile was predicted by *in silico* approach.

2. Experimental

2.1. Materials and physical measurements

All chemicals were of reagent grade and used as commercially purchased without further purification. The elemental analyses were determined by a Thermo-Finnigan Flash EA 1112 Series Elementary Analyzer. ^{1}H-NMR spectra were recorded on a Bruker Avance-500 model spectrometer relative to $SiMe_4$ using deuterated chloroform as solvent at 25 ± 2 °C.

2.2. Synthesis

2.2.1. S-propyl-N[1]-2-amino-3,5-dibromobenzylidene thiosemicarbazone

The thiosemicarbazone compound as the starting material was synthesized in the same way as that in our previous study (Şahin et al., 2020). About 0.45 g thiosemicarbazide (5 mmol) and 0.45 mL 1-bromopropane (5 mmol) were mixed in 15 mL ethanol. The mixture was refluxed for 3 h. Then, 1.39 g (5 mmol) 2-amino-3,5-dibromo benzaldehyde was solved in ethanol/chloroform (1:1; 10 mL) and added to reaction medium. The reaction mixture was refluxed for 4 h, and the clear solution was cooled. The hydrobromide form of the thiosemicarbazone was neutralized with a sufficient amount of aqueous $NaHCO_3$ solution. The separated yellow precipitate, was filtered off, washed with water and cold ethanol. The colour, m.p. (°C), yields (%) and the elemental analysis of the data are given as follows: Yellow, 155 °C, 66%, Anal. Found (Calc.) for $C_{11}H_{14}Br_2N_4S$ (394.13 g/mol) C, 33.50 (33.52); H, 3.60 (3.58); N, 14.20 (14.22); S, 8.00 (8.14)%.

2.2.2. N_1-2-amino-3,5-dibromobenzylidene-N_4-2-amino-3,5-dibromobenzylidene-S-propyl thiosemicarbazidato-nickel(II) (NiL)

About 0.24 g (1 mmol) $NiCl_2{\cdot}6H_2O$ was dissolved in 15 mL absolute ethanol. A solution of 0.39 g (1 mmol) *S*-propyl-N[1]-amino-3,5-dibromobenzylidene thiosemicarbazone and 0.28 g (1 mmol) 2-amino-3,5-dibromo benzaldehyde in ethanol/chloroform (1:4; 20 ml) was added drop wise to the metal solution with vigorous stirring. The dark red coloured reaction mixture was stirred at 45 °C for 3 h and then allowed to stand at room temperature. After addition of triethylamine (0.1 mmol), the mixture was left to stand at room temperature for a few days. The brown product was collected by filtration and washed with cold chloroform (Figure 1). Recrystallization of the product from ethanol/chloroform mixture gave the analytical grade pure NiL complex. The colours, m.p. (°C), yields (%) and the elemental analysis of the data are given as follows: Brown, 277 °C; 38%, Anal. Found (Calc.) for $C_{18}H_{15}Br_4N_5NiS$ (711.72 g/mol): C, 30.24 (30.38); H, 2.16 (2.12); N, 9.76 (9.84); S, 4.42 (4.51) %.

2.3. Experimental and computational studies

The Spartan06 program (Shao et al., 2006) was used to determine the most stable conformation of NiL using density functional theory (DFT)/B3LYP calculation method, 6-311++G(d, p) basis set (Becke, 1993). The obtained stable geometry was used as initial geometry and the lowest molecular energy was then calculated using the (DFT)/B3LYP/311++G(d, p) level of theory by Gaussian03 software (Frisch et al., 2004). Figure 2 shows the optimized geometric structures of the title molecule using the theory level of DFT/B3LYP/6-311++G(d, p).

The harmonic force field for the title molecule was determined using Pulay et al. (1983) scaled quantum mechanical force field treatment. The transformation of force field from Cartesian to internal coordinates, calculation of potential energy distribution (PED) and prediction of IR and Raman intensities of the vibration modes was done by using the Molvib program (Sundius, 1990, 2002). The Raman intensity was evaluated using the simulation software Simirra which transformed Raman activities into intensity (Istvan, 2002). The simulations used Lorentzian band shapes with bandwidth (FWHM) of 10 cm^{-1}.

The scale factors of N–H stretch, C–H stretch, N–H deformations, C–H deformations and all others were chosen as 0.89, 0.91, 0.92, 0.92 and 0.98, respectively to give the best fit to the experimental data.

3. Results and discussion

3.1. Structural parameters and vibrational analysis

The structural parameters of the lowest-energy conformer of NiL complex are tabulated in Table 1, in comparison with the crystal data of *N_1-2-hydroxy-5-bromobenzylidene-N_4-2-amino-3,5-dibromobenzylidene-S-propylthiosemicarbazidato Nickel(II)* (Complex **1a**), taken from Şahin et al. (2020). As seen in Table 1, the calculated molecular parameters of the title molecule are compatible with the experimental parameters of the crystal structure of Complex **1a** (Şahin et al., 2020). Moreover, in supplemental file Figure S1 the most stable molecular structure of NiL complex and the crystallographic structure of Complex **1a** (Şahin et al., 2020) are shown comparatively which shows that the structure of the title molecule is analogous to complex **1a**.

The NiL molecule contains 44 atoms and therefore has 126 normal modes of vibration. The calculated harmonic vibrational wavenumbers of the most stable conformer of NiL together with the experimental FTIR and Raman vibrational wavenumbers, and their tentative vibrational assignments are presented in Table 2. These assignments were done based on calculated PEDs of the vibrational modes. In Table 2 only contributions to PED equal to or greater than 5 were included.

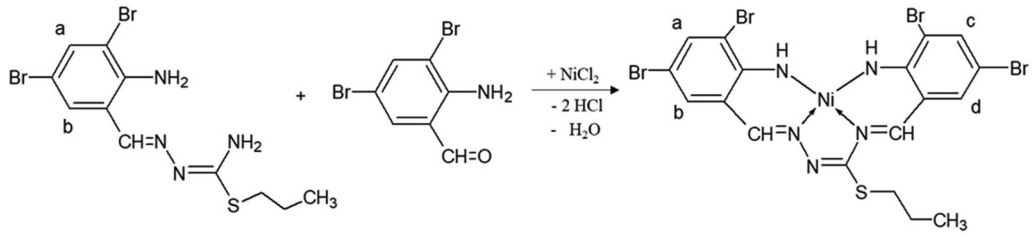

Figure 1. The formation of the complex [**NiL**].

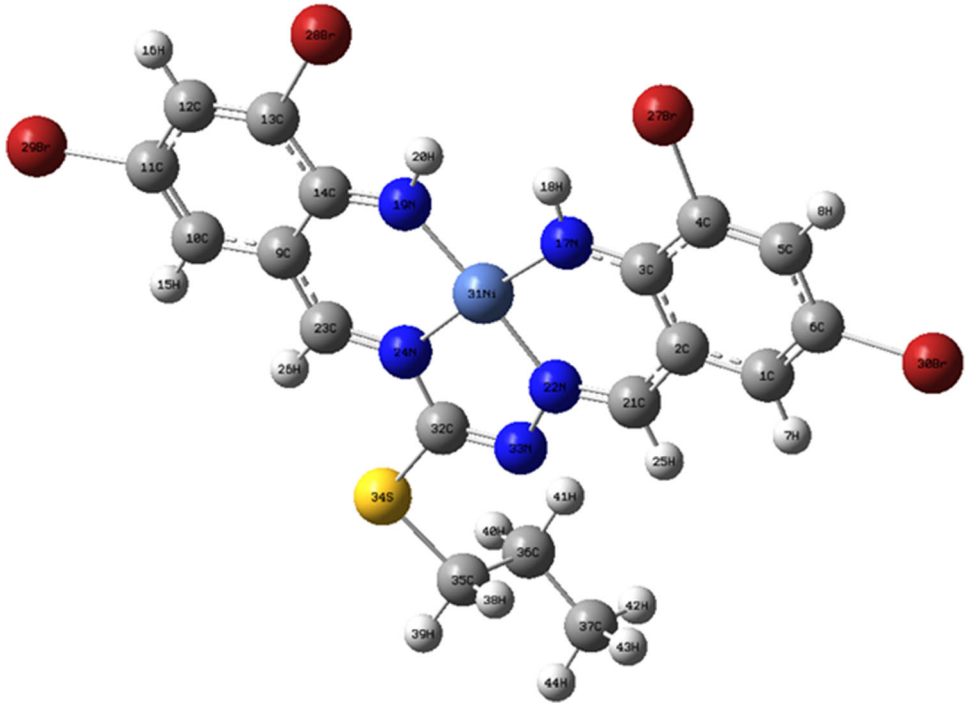

Figure 2. The most stable molecular structure of NiL calculated by DFT/B3LYP/6-311++G(d, p).

Table 1. The structural parameters of NiL obtained by DFT/B3LYP (6-311++G(d, p)), compared to experimental data of complex **1a**.

Atoms[a]	NiL	Complex **1a**[b]	Atoms[a]	NiL	Complex **1a**[b]	Atoms[a]	NiL	Complex **1a**[b]	Atoms[a]	NiL	Complex **1a**[b]
R(1,2)	1.418	1.4	R(17,31)	1.866		A(6,1,7)	120.5	118.7	A(11,12,13)	119.9	121.4
R(1,6)	1.369	1.37	R(19,20)	1.015	0.86	A(1,2,3)	120.9	121.4	A(11,12,16)	119.9	119.4
R(1,7)	1.083	0.93	R(19,31)	1.868	1.85	A(1,2,21)	117.5	117.2	A(13,12,16)	120.2	119.1
R(2,3)	1.443	1.43	R(21,22)	1.309	1.31	A(3,2,21)	121.6	121.2	A(12,13,14)	123.1	123.5
R(2,21)	1.416	1.39	R(21,25)	1.087	0.93	A(2,3,4)	115.0	116.3	A(12,13,28)	118.3	116.8
R(3,4)	1.438	1.46	R(3,17)	1.331		A(2,3,17)	122.0		A(14,13,28)	118.6	119.7
R(22,31)	1.863	1.89	R(22,33)	1.384	1.42	A(4,3,17)	123.0		A(9,14,13)	115.1	114.6
R(4,5)	1.371	1.43	R(23,24)	1.322	1.38	A(3,4,5)	123.3	119.6	A(9,14,19)	122.0	122.8
R(4,27)	1.922		R(23,26)	1.088	0.93	A(3,4,27)	118.6		A(13,14,19)	122.9	122.6
R(5,6)	1.410	1.4	R(24,31)	1.886	1.86	A(5,4,27)	118.1		A(3,17,18)	112.0	
R(5,8)	1.082	0.93	R(24,32)	1.397	1.38	A(4,5,6)	119.7	120.9	A(3,17,31)	130.0	
R(6,30)	1.916	1.88	R(32,33)	1.293	1.29	A(4,5,8)	120.2	120	A(18,17,31)	118.0	
R(9,10)	1.425	1.42	R(32,34)	1.774	1.76	A(6,5,8)	120.1	119.1	A(14,19,20)	112.0	114.9
R(9,14)	1.449	1.45	R(34,35)	1.839	1.8	A(1,6,5)	120.3	119.5	A(14,19,31)	130.1	130.1
R(9,23)	1.405	1.38	R(35,36)	1.528	1.39	A(1,6,30)	120.7	123.4	A(20,19,31)	117.9	115
R(10,11)	1.363	1.43	R(35,38)	1.090	0.97	A(5,6,30)	119.0	117.1	A(2,21,22)	125.1	124.9
R(10,15)	1.083	0.93	R(35,39)	1.093	0.97	A(10,9,14)	120.6	123.3	A(2,21,25)	118.7	117.6
R(11,12)	1.417	1.46	R(36,37)	1.533	1.4	A(10,9,23)	117.3	114.9	A(22,21,25)	116.2	117.5
R(11,29)	1.915	1.81	R(36,40)	1.094	0.97	A(14,9,23)	122.1	121.8	A(21,22,31)	128.7	126
R(12,13)	1.366	1.38	R(36,41)	1.092	0.98	A(9,10,11)	120.8	120	A(21,22,33)	115.3	119.3
R(12,16)	1.082	0.93	R(37,42)	1.093	0.96	A(9,10,15)	118.6	119.9	A(31,22,33)	116.0	114.7
R(13,14)	1.445	1.43	R(37,43)	1.094	0.96	A(11,10,15)	120.5	120.2	A(9,23,24)	125.7	126
R(13,28)	1.919	1.9	R(37,44)	1.095	0.96	A(10,11,12)	120.4	116.6	A(9,23,26)	116.3	117.3
R(14,19)	1.323	1.3	A(3,17,31)	130.0		A(10,11,29)	120.9	121.7	A(24,23,26)	118.0	116.6
R(17,18)	1.014		A(19,31,17)	91.7		A(12,11,29)	118.7	121.6	A(2,1,7)	118.7	119.2

[a]R and A stand for bond (Å), angle (deg), respectively.
[b]Crystallographic data of complex **1a** = N_1-2-hydroxy-5-bromobenzylidene-N_4-2-amino-3,5-dibromobenzylidene-*S*-propylthiosemicarbazidato Nickel(II), taken from Şahin et al. (2020).

Table 2. The calculated (B3LYP/6-311++G(d, p)) and experimental wavenumbers (cm^{-1}) of NiL and the PED distributions of the vibration modes.

Experimental		Calculated B3LYP/6-311++G(d,p)			
FTIR	Raman	ν_{cal}*	I(IR)	I(Ra)	PED % (≥5)
		3335	22	1	ν_{NH}(98)
3316		3325	39	1	ν_{NH}(98)
		3063	2	1	ν_{CH}(99)
3060		3063	2	1	ν_{CH}(99)
		3045	1	1	ν_{CH}(99)
		3044	2	1	ν_{CH}(99)
3005		3004	4	1	ν_{CH}(99)
		2989	2	1	ν_{CH}(99)
		2978	7	0	ν_{CH}(92)
2958		2950	31	1	ν_{CH}(92)
		2949	35	1	ν_{CH}(93)
		2929	5	1	ν_{CH}(87)
2922		2915	17	2	ν_{CH}(95)
2871		2898	10	1	ν_{CH}(94)
2851		2882	35	2	ν_{CH}(99)
		1615	225	2	ν_{CC}(31)+ ν_{CN}(13)
		1605	475	4	ν_{CN}(20)+ ν_{CC}(29)
1590	1590	1596	74	7	ν_{CN}(26)+ ν_{CC}(42)
1569	1575	1587	324	6	ν_{CN}(31)+ ν_{CC}(29)+ δ_{CCH}(7)+ δ_{NCH}(6)
		1542	75	100	ν_{CN}(45)
1525	1523	1514	25	19	ν_{CN}(22)+ ν_{CC}(23)+ δ_{CNH}(6)
1499	1501	1506	306	12	ν_{CC}(34)+ δ_{CNH}(5)
		1468	120	72	ν_{CN}(16)+ δ_{HCH}(14)+ ν_{CC}(6)
		1466	194	76	ν_{CN}(30)+ ν_{CC}(19)
1456		1454	7	27	δ_{HCH}(63)+ δ_{CCH}(5)+ Γ_{HCCH}(6)
		1453	1	27	ν_{CN}(37)+ ν_{CC}(23)
	1445	1452	3	25	δ_{HCH}(42)+ Γ_{HCCH}(7)
1425		1424	13	5	ν_{CC}(50)+ ν_{CN}(9)
		1418	8	8	δ_{HCH}(18)+ ν_{CC}(16)+ δ_{CNH}(6)
	1415	1414	66	7	ν_{CC}(25)+ ν_{CN}(12)+ δ_{HCH}(7)+ δ_{CNH}(5)
1404	1396	1402	18	16	ν_{CC}(39)+ ν_{CN}(8)+ δ_{CCH}(7)
		1380	13	2	ν_{CC}(43)+ δ_{CNH}(5)
1361	1365	1363	6	7	δ_{NCH}(18)+ δ_{CCH}(15)+ δ_{CNH}(6)+ ν_{CN}(5)
		1360	47	9	ν_{CN}(10)+ δ_{NCH}(7)+ δ_{CNH}(5)
		1356	2	5	δ_{CCH}(54)+ ν_{CC}(13)+ δ_{HCH}(22)
		1336	7	5	ν_{CC}(24)+ δ_{CCH}(37)
	1331	1332	4	8	δ_{CNH}(14)+ δ_{CCH}(8)+ δ_{NiNH}(8)+ ν_{CC}(8)+ ν_{CN}(7)+ δ_{NCH}(6)
		1321	4	2	ν_{CC}(15)+ δ_{CCH}(17)+ ν_{CN}(7)
1318		1312	33	1	δ_{CCH}(29)+ ν_{CC}(19)+ δ_{NCH}(6)
	1304	1296	9	2	δ_{CNH}(14)+ δ_{NCH}(11)+ δ_{CCH}(23)+ δ_{NiNH}(10)
		1282	1	1	δ_{CCH}(73)
	1239	1244	13	3	δ_{CCH}(30)+ δ_{SCH}(30)
		1234	24	9	δ_{CCH}(42)+ ν_{CN}(15)+ ν_{CC}(7)
1213	1214	1217	6	2	δ_{CCH}(58)
	1193	1210	195	3	δ_{CCH}(38)+ ν_{CC}(19)+ δ_{NCH}(7)
		1155	613	9	ν_{CN}(32)+ ν_{CS}(11)+ ν_{CC}(8)+ δ_{NCN}(5)
1147	1146	1141	167	4	ν_{CC}(30)+ δ_{CCH}(6)
	1136	1133	83	2	ν_{CC}(30)+ δ_{CCH}(6)
1095	1098	1098	2	3	ν_{CC}(40)+ δ_{CCH}(29)+ ν_{CBr}(9)
		1089	62	6	ν_{CC}(43)+ ν_{CBr}(10)+ δ_{CCH}(21)
	1081	1085	34	5	ν_{CC}(47)+ δ_{CCH}(23)
1076	1073	1067	17	25	δ_{SCH}(23)+ ν_{NN}(11)+ δ_{CCH}(20)
		1053	49	70	ν_{NN}(52)
1028	1027	1019	0	2	ν_{CC}(93)
		949	11	1	Γ_{HCNN}(31)+ Γ_{CCCH}(40)+ Γ_{HCNNi}(12)
	947	948	16	1	δ_{CCC}(15)+ ν_{CBr}(15)
		937	8	2	Γ_{HCNC}(18)+ Γ_{CCCH}(26)+ Γ_{HCNNi}(8)
936		936	15	2	δ_{CCC}(30)+ ν_{CBr}(17)
	896	896	7	3	Γ_{HCCBr}(50)+ Γ_{CCCH}(33)
		894	29	3	ν_{CS}(16)+ δ_{NNC}(9)+ δ_{NCN}(6)
		892	5	3	Γ_{BrCCH}(46)+ Γ_{CCCH}(37)
881		885	7	1	ν_{CC}(58)+ δ_{CCH}(25)+ ν_{CS}(5)
		866	17	1	Γ_{BrCCH}(40)+ Γ_{CCCH}(41)
		864	13	1	Γ_{BrCCH}(29)+ Γ_{CCCH}(44)
858	851	849	13	9	ν_{CC}(28)+ ν_{NNi}(7)+ ν_{CBr}(7)
		835	3	2	δ_{CCH}(39)
		833	10	2	ν_{CC}(20)+ ν_{CBr}(5)
755		747	16	0	Γ_{CCNH}(13)+ Γ_{BrCCN}(10)+ Γ_{CCCC}(16)+ Γ_{CCCN}(8)+ Γ_{CCNNi}(7)
743		739	7	0	Γ_{BrCCN}(10)+ Γ_{CCCC}(24)+ Γ_{CCCN}(9)+ Γ_{CCNH}(7)
		725	10	1	ν_{CS}(7)+ Γ_{HCCH}(11)

(*continued*)

Table 2. Continued.

Experimental		Calculated B3LYP/6-311++G(d,p)			
FTIR	Raman	ν_{cal}*	I(IR)	I(Ra)	PED % (≥5)
722		721	38	2	$\nu_{NNi}(25)+ \nu_{CBr}(15)$
	712	712	6	2	$\nu_{CBr}(18)$
708		708	31	3	$\nu_{CBr}(21)+ \nu_{CC}(5)$
		704	47	3	$\nu_{CS}(19)+ \nu_{CBr}(24)$
		701	39	3	$\Gamma_{HNNiN}(43)+ \Gamma_{CCNH}(38)$
		698	17	3	$\nu_{CS}(44)$
680	684	683	19	2	$\nu_{CS}(6)+ \nu_{NNi}(12)+ \delta_{CNC}(6)$
650	649	649	40	3	$\delta_{CNNi}(9)+ \nu_{NNi}(7)$
628		633	0	1	$\Gamma_{NCNN}(16)+ \Gamma_{NiNCN}(13)+ \Gamma_{CNCS}(8)+ \Gamma_{NiNNC}(6)+ \Gamma_{NCSC}(5)+ \Gamma_{CCNH}(5)$
599		613	7	0	$\Gamma_{CCNH}(43)+ \Gamma_{HNNiN}(32)$
	568	575	2	6	$\nu_{NNi}(18)+ \delta_{CCC}(6)+ \delta_{NiNN}(5)$
		560	2	2	$\nu_{NNi}(33)+ \nu_{CS}(10)$
		546	2	0	$\Gamma_{CCCC}(34)+ \Gamma_{CCCH}(22)$
543		540	2	0	$\Gamma_{CCCC}(34)+ \Gamma_{CCCH}(24)$
521	518	512	46	3	$\nu_{CS}(26)+ \nu_{NNi}(19)+ \delta_{NCS}(5)$
503		507	9	1	$\Gamma_{CCCC}(6)+ \Gamma_{NCCBr}(6)$
485		487	0	0	$\Gamma_{CCCC}(7)+ \Gamma_{CCCH}(5)$
		458	3	1	$\nu_{NNi}(16)+ \delta_{CSC}(13)+ \delta_{CCC}(6)$
459	455	452	2	1	$\Gamma_{HCNNi}(11)+ \Gamma_{NiNNC}(9)+ \Gamma_{CCNNi}(9)+ \Gamma_{NNNiN}(6)$
428		433	0	0	$\nu_{NNi}(22)+ \delta_{CCBr}(15)$
	405	404	2	3	$\nu_{NNi}(25)+ \delta_{CBr}(9)$
		387	0	1	$\nu_{NNi}(6)$
		375	1	1	$\Gamma_{CCNNi}(9)+ \Gamma_{HCNNi}(7)$
		367	3	1	$\nu_{CS}(16)+ \delta_{CCC}(12)+ \delta_{CCS}(7)$
	355	351	4	2	$\nu_{CBr}(24)+ \nu_{NNi}(7)+ \nu_{CS}(6)$
		349	4	2	$\nu_{CBr}(5)$
		332	2	1	$\Gamma_{CCCN}(16)+ \Gamma_{CCNNi}(7)+ \Gamma_{BrCCC}(6)+ \Gamma_{BrCCH}(6)+ \Gamma_{CNNiN}(6)$
		329	1	1	$\nu_{CBr}(27)+ \nu_{CS}(8)+ \delta_{CSC}(8)$
	325	323	0	2	$\nu_{CBr}(17)+ \delta_{CSC}(8)+ \delta_{CS}(6)$
		307	0	0	$\Gamma_{BrCCC}(14)+ \Gamma_{CCCN}(12)+ \Gamma_{BrCCH}(12)$
		292	2	0	$\nu_{CBr}(39)$
		253	1	1	$\delta_{CCC}(7)+ \delta_{SCC}(6)$
		249	0	1	$\Gamma_{HCCH}(34)+ \Gamma_{CCCH}(16)$
		230	1	2	$\Gamma_{CCCH}(31)+ \Gamma_{HCCH}(30)$
	232	228	1	2	$\nu_{CBr}(19)+ \Gamma_{CCCH}(19)+ \Gamma_{HCCH}(6)$
		222	1	3	$\delta_{CSC}(9)+ \delta_{SCC}(8)+ \nu_{CBr}(11)$
		218	0	3	$\delta_{SCC}(15)+ \delta_{CCC}(6)+ \delta_{CSC}(6)$
	188	190	2	8	$\delta_{CSC}(12)+ \nu_{CBr}(6)$
		172	0	2	$\Gamma_{BrCCC}(9)$
	161	153	0	4	$\Gamma_{CNNiN}(29)+ \Gamma_{CCNNi}(11)$
		142	0	9	$\Gamma_{BrCCC}(17)+ \Gamma_{BrCCN}(7)$
		141	1	10	$\delta_{CCBr}(6)$
	136	137	1	10	$\delta_{CCBr}(24)+ \delta_{NCS}(5)$
	121	120	0	3	$\Gamma_{CSCH}(20)+ \Gamma_{CSCC}(10)$
	105	105	1	9	$\delta_{CCBr}(43)$
		101	0	11	$\Gamma_{BrCCC}(5)$
		100	0	10	$\delta_{CCBr}(57)$
		92	0	5	$\nu_{NNi}(7)+ \delta_{CCBr}(11)$
		77	0	3	$\Gamma_{CSCH}(19)+ \Gamma_{CSCC}(9)+ \Gamma_{SCCH}(15)+ \Gamma_{SCCC}(8)$
	56	60	0	6	$\Gamma_{CCNNi}(6)+ \Gamma_{NCSC}(5)$
		46	0	10	$\Gamma_{SCCC}(9)+ \Gamma_{SCCH}(16)+ \Gamma_{CCCH}(15)+ \Gamma_{HCCH}(8)$
		43	0	12	$\Gamma_{SCCC}(7)+ \Gamma_{SCCH}(13)+ \Gamma_{CCCH}(12)+ \Gamma_{HCCH}(6)$
		33	0	19	$\Gamma_{SCCC}(7)+ \Gamma_{SCCH}(13)+ \Gamma_{CCCH}(6)+ \Gamma_{HCCH}(12)$
		14	0	102	$\Gamma_{HNNiN}(24)+ \Gamma_{CNNiN}(6)$
		11	0	128	$\Gamma_{CNCS}(7)+ \Gamma_{CNNiN}(6)+ \Gamma_{NCSC}(11)+ \Gamma_{CNCN}(5)$
		10	0	125	$\Gamma_{NCSC}(62)+ \Gamma_{CSCC}(7)+ \Gamma_{CSCH}(13)$

Figures 3 and 4 show comparisons of the theoretical IR and Raman spectra with the experimental NiL spectra. Since the original Raman spectrum of NiL has high background due to fluorescence, baseline corrected Raman spectrum is given in Figure 4 and the original Raman spectrum is given as the supplemental file (Figure S2).

The experimental and calculated vibrational wavenumber fit was also analysed. The mean absolute deviation, standard deviation, root mean square and correlation coefficient (*r*) between the calculated and observed vibrational frequencies of the NiL are given in Table 3.

The N–H stretching vibrations of occur within the range of 3500–3000 cm^{-1}. In a research on Gly-Tyr performed by Celik et al. (2017) these modes were observed in the 3326–3210 cm^{-1} spectral range. In another study performed by Sadler (1961) on the 3-thiosemicarbazone, the 3-4′-phenylthiosemicarbazone, and the 3-4′,4′-dimethylthiosemicarbazone of 1-methylisatin, the N–H stretching modes were reported at 3400 and 3200 cm^{-1}. In this study, N–H stretching modes were evaluated at 3335 and 3325 cm^{-1} in accordance with previous studies and observed at 3316 cm^{-1}.

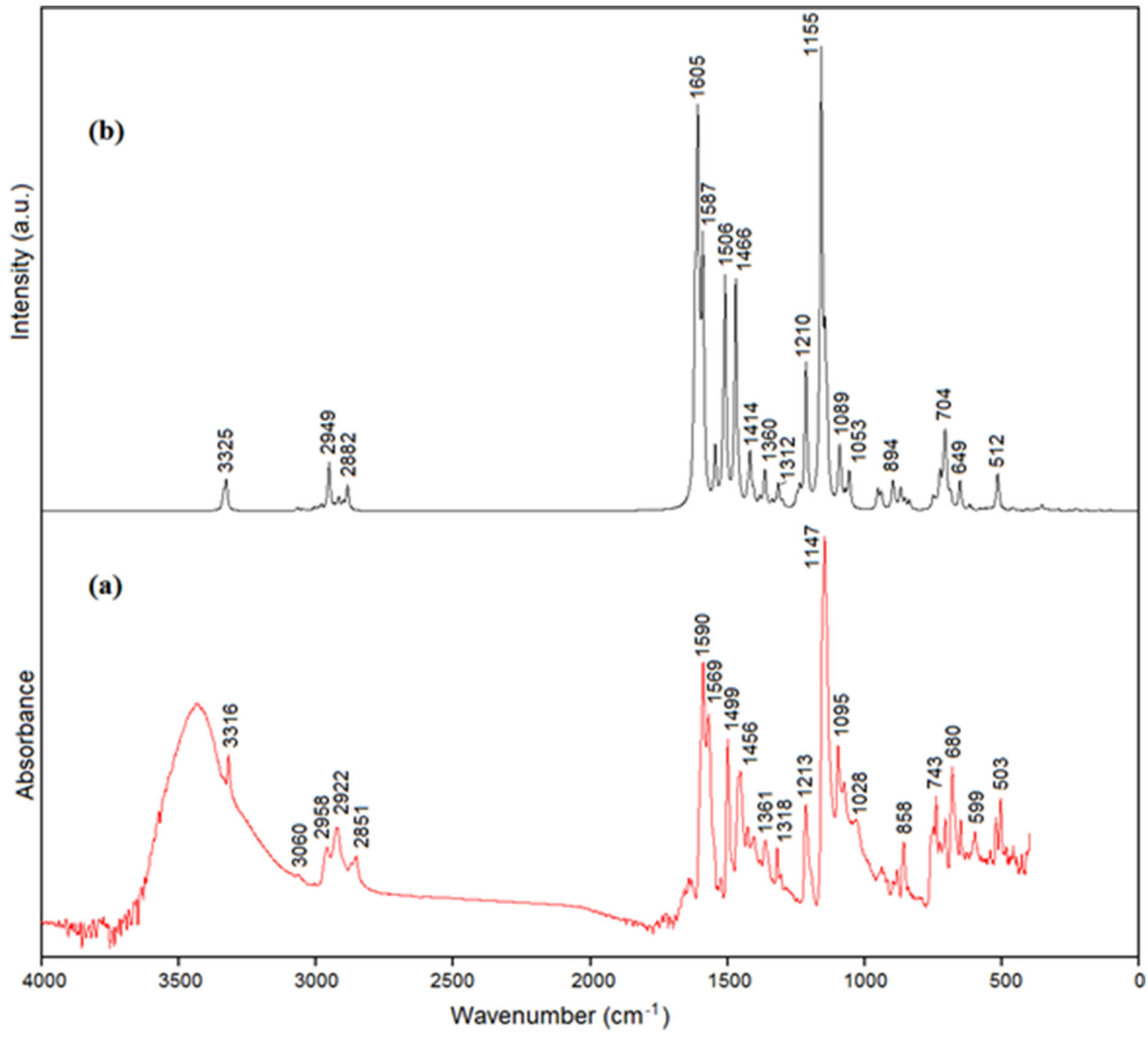

Figure 3. The experimental (a), and calculated (b) IR spectra of the NiL (b).

The typical range for C–H stretching vibrations is 3100–2800 cm^{-1}. The C–H stretching modes were calculated around 3110–2911 cm^{-1} (Singh & Singh, 2015) for the 2-acetylpyridine thiosemicarbazone. In a study on 4-(3-fluorophenyl)-1-(propan-2-ylidene)-thiosemicarbazone (Sert et al., 2014), the C–H stretching modes were observed in the range of 3166–2857 cm^{-1} in the FT-IR spectrum. The aliphatic C–H stretching modes were estimated by (Celik, Albayrak, Akyuz, & Ozel, 2019) using DFT/wb97xd/6-31G(d,p) method in the range of 3069–2893 cm^{-1}. In our study these vibrations were calculated around 3063–2882 cm^{-1} and observed 3060–2851 cm^{-1} in the FTIR spectrum.

The CNH bending vibrational mode wavenumbers for NiL molecule were calculated as 1332 cm^{-1} and the Raman spectrum were observed at 1331 cm^{-1}. This results are in agreement with the study on zinc(II) and mercury(II) complexes of isatin-3-thiosemicarbazone (ISTSCH) in which were observed as 1348 (ISTSCH), 1398 (zinc complex) and 1347 cm^{-1} (mercury complex) in the IR spectra (Akinchan et al., 2002).

The stretching vibration of C–Br normally occurs at area 650–200 cm^{-1} (Griffiths & Thompson, 1967; Singh & Shamir, 1977; Suzuki, 1977; Varsanyi, 1974, 2012). The calculated values corresponding to C–Br stretching modes are at 351, 329, 292 and 228 cm^{-1}, with PED contributions of 24%, 27%, 39% and 19%, respectively. This mode was observed at 405 $cm^{-1}$by Das et al. (2018) in the IR spectrum of (E)-1-(4-bromobenzylidene) thiourea.

N–N stretching mode, which was calculated as 1044 cm^{-1} by Bharanidharan et al. (2017) for (E)-*N*′-(thiophen-2-ylmethylene) Nicotinohydrazide, was calculated as 1053 cm^{-1} in this study.

In a study on the Ni(II) thiosemicarbazone ligands and complexes, connected by Shawish and Bashir (2014), the N–Ni stretching modes were observed in the range of 531–565 cm^{-1}. In this study the N–Ni stretching modes were calculated as 575, 560, 433 and 404 cm^{-1} and were observed at 568 and 405 cm^{-1} in the Raman spectrum.

3.2. Molecular electrostatic potential (MEP)

In Figure 5 the MEP surface of the NiL, changing from −0.566 V (darkest red) to 0.566 V (deepest blue), is shown. The blue colour indicates nucleophilicity, while the red colour indicates electrophilicity. The map of MEP shows the regions with negative potential are on bromine and the

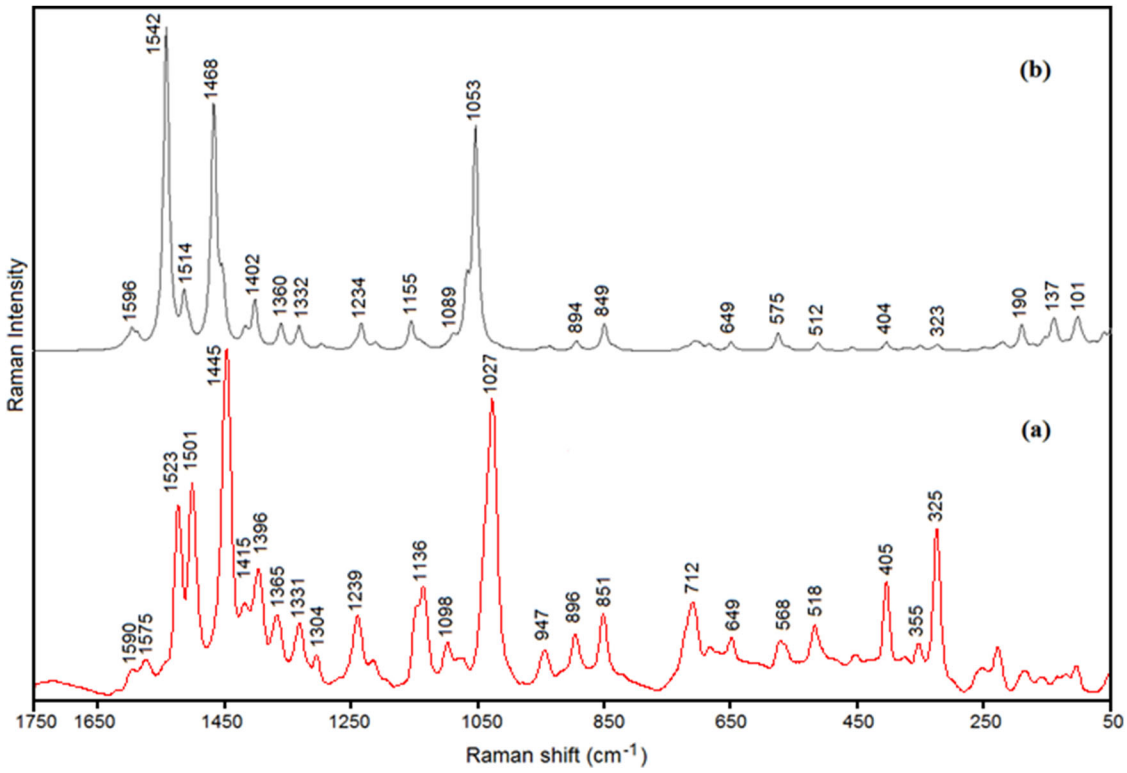

Figure 4. The experimental (a) and calculated (b) Raman spectra of NiL in the region of 1750–50 cm^{-1}.

Table 3. Mean absolute deviation, standard deviation, root mean square and correlation coefficient (*r*) between the calculated and observed vibrational frequencies of the NiL.

Parameter	IR B3LYP/6-311++G(d, p)	Raman B3LYP/6-311++G(d, p)
Mean absolute deviation	6.605	4.079
Standard deviation	4.714	2.772
Root mean square	8.365	4.918
Correlation coefficient	0.99995	0.99994

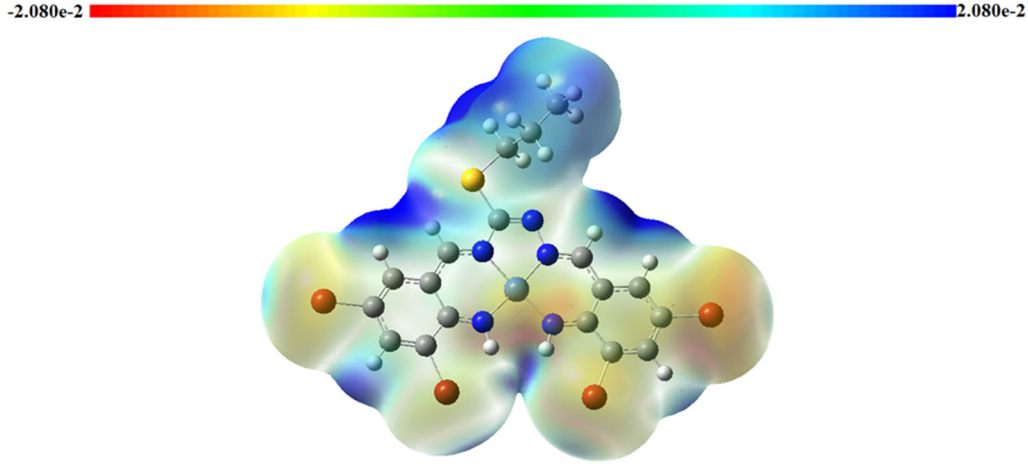

Figure 5. Molecular electrostatic potential (MEP) of NiL obtained by DFT/B3LYP/6-311++G(d, p) method using GaussView.

hydrogen atoms of the NH and CH groups are located in regions with positive potential.

3.3. Highest occupied molecular orbital (HOMO) and lowest occupied molecular orbital (LUMO) energies

Highest occupied molecular orbital (HOMO) and lowest occupied molecular orbital (LUMO) energies, which are the measures of the kinetic stability and reactivity of the compounds, are calculated for NiL by DFT method at the theoretical level of B3LYP/6-311++G(d,p). The smaller the energy gap between HOMO and LUMO energies is the more reactive is the molecule (Pearson, 1973). Sens et al. (2018) calculated the HOMO–LUMO energy gap of a series TSC, in the 1.421–5.658 eV range. Smaller HOMO–LUMO energy gap can be indicative of a greater biological activity (Patra et al., 2018).The HOMO–LUMO energy separation of the title compound was found to be 2.585 eV (0.095 a.u.). This value

describes the probable charge transfer interaction within the molecule, which determines the biological activity of the compound. The frontier molecular orbitals (HOMO and LUMO) are shown in Figure 6.

3.4. Analysis of toxicological and physicochemical properties

The estimated toxicity risk values and some significant physicochemical properties of NiL were determined using OSIRIS Property Explorer (2010).The results are given in Table 4. The clogP, value of a compound, which is the logarithm of its partition coefficient between *n*-octanol and water $\log(c_{octanol}/c_{water})$, is used as a measure of the hydrophilicity of a compound. In other words, cLogP is a measure of molecular hydrophobicity, between *n*-octanol and water. Compounds that have high hydrophobicity property and therefore high clogP values show poor absorption or permeation property. The cLogP was estimated as a 5.77 for the title molecule. Whether the target molecule has a value below 5 shows the probability that it can be well absorbed (Molinspiration Cheminformatics, n.d.; OSIRIS Property Explorer, 2010). Log S which represents the solubility of the drug is an important factor and is greater than –4 for common commercial drugs. Poor solubility → poor absorption → bioavailability. In this study, this value of the NiL examined is –8.49. The molecular weight is an identifier of absorption. More than 80% of all commercial drugs have a molecular weight below 450 (OSIRIS Property Explorer, 2010) however the value of NiL is 709. In addition, the total polar surface area (TPSA), intestinal absorption, bioavailability, Caco-2 permeability and blood–-brain barrier (BBB) penetration are also other good identifiers of absorption. (Ertl et al., 2000). The combination of drug likeness, cLogP, log S, molecular weight and toxicity risks form the drug score (DS) (OSIRIS Property Explorer, 2010).

3.5. Absorption analysis of target NiL

The BBB is the brain's microvascular endothelial cell layer which plays a key role in keeping the brain away from the blood and protects the brain from exogenous compounds. The high BBB entrance is required for the majority of the medications focusing on the central nervous system (CNS), though for non-CNS tranquilizes the BBB infiltration ought to be limited, to keep away from undesired symptoms (Bemis & Murcko, 1999). The intestinal absorption values are in the range of 0–20% for poorly absorbed compounds, 20–70% for moderately absorbed compounds and 70–100% for well absorbed compounds. The NiL demonstrated a positive intestinal absorption values which could be ingested by human intestine (Yee, 1997; Zhao et al., 2001). Caco-2 permeability is used in the drug selection process to monitor intestinal absorption and is a culture of human colon epithelial cancer cells widely used for the assimilation of drugs and other compounds in the human intestine. (Lea et al., 2015; Yamashita et al., 2000). NiL showed a negative result in Caco2 permeability, which showed that it was not permeable. P-gp molecules avoid the entry of antimicrobials into

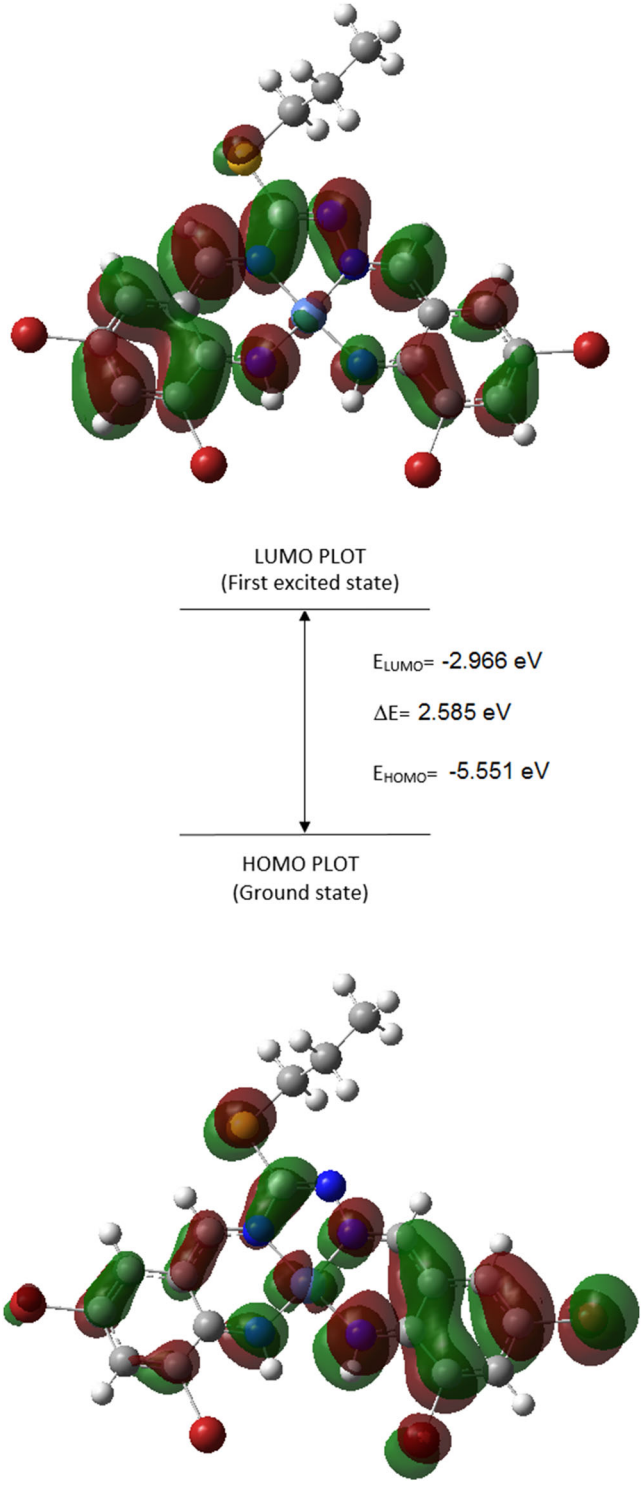

Figure 6. HOMO-LUMO composition for NiL.

the microorganisms and as with the enzymes involved in drug metabolism, P-glycoprotein substrates may serve as inhibitors or inducers of its function (Amin, 2013). In addition, inhibition of P-glycoprotein may cause increased bioavailability of the susceptible drug, and induction of P-glycoprotein has been shown to reduce bioavailability (Finch & Pillans, 2014).

The cytochrome P450 monooxygenase enzymes (P450s) facilitate a diverse array of chemical transformations, due to the insertion of an oxygen atom to a substrate which binds

Table 4. Osiris's estimation of title compounds toxicity hazards and physicochemical properties.

	Toxicity risks				Physicochemical properties					
Compound	Mutagenic	Tumorigenic	Irritant	Reproductive Effect	CLogP	Solubility	MW	TPSA	Drug likeness	Drug score
NiL	Medium risk	Medium risk	High risk	Medium risk	5.77	−8.49	709	68.2	−5.17	0.03

Table 5. Prediction of ADMET profiles of the NiL.

Human intestinal absorption	+	0.9893
ADMET predicted profile—classifications value probability		
Caco-2	−	0.6297
Blood–brain barrier	+	0.9756
Human oral bioavailability	+	0.5429
Subcellular localization	Mitochondria	0.4347
OATP2B1 inhibitor	−	1.0000
OATP1B1 inhibitor	+	0.8901
OATP1B3 inhibitor	+	0.9370
MATE1 inhibitor	−	0.9000
OCT2 inhibitor	−	0.6500
BSEP inhibitor	+	0.9165
P-glycoprotein inhibitor	+	0.6188
P-glycoprotein substrate	+	0.6453
CYP3A4 substrate	+	0.6082
CYP2C9 substrate	−	0.5948
CYP2D6 substrate	−	0.7746
CYP3A4 inhibition	+	0.7155
CYP2C9 inhibition	−	0.5679
CYP2C19 inhibition	+	0.5483
CYP2D6 inhibition	−	0.8056
CYP1A2 inhibition	+	0.5181
CYP inhibitory promiscuity	+	0.9568
UGT catalyzed	−	0.0000
Carcinogenicity (binary)	−	0.8000
Carcinogenicity (trinary)	Non-required	0.5595
Eye corrosion	−	0.9764
Eye irritation	−	0.9447
Ames mutagenesis	−	0.7200
Human either-a-go-go inhibition	+	0.8980
Micronuclear	+	0.8500
Hepatotoxicity	+	0.6250
Acute Oral Toxicity (c)	III	0.5602
Oestrogen receptor binding	+	0.7065
Androgen receptor binding	+	0.7764
Thyroid receptor binding	+	0.5720
Glucocorticoid receptor binding	+	0.6719
Aromatase binding	+	0.8131
PPAR gamma	+	0.8369
Honey bee toxicity	−	0.5773
Biodegradation	−	0.8000
Crustacea aquatic toxicity	+	0.6300
Fish aquatic toxicity	+	0.9921
ADMET predicted profile—Regressions	Value	Unit
Water solubility	−3.606	logS
Plasma protein binding	1.006	100%
Acute oral toxicity	2.978	kg/mol
Tetrahymena pyriformis	2.274	pIGC50 (ug/L)

close to the P450 heme. Cytochrome P450 inhibitors are also an effective detoxification enzyme, which is commonly found in the body's liver (Sheweita, 2000; Zanger & Schwab, 2013).hERG (ion channels) which contribute to the electrical activity of the heart, mediates the repolarizing IKr current to coordinate the heart's beating. When this channel's ability is inhibited because of the Mutations or othervarious interactions, hERG conductivity can reduce and it can result in a potentially fatal disorder called long QT syndrome (Piippo et al., 2000; Tristani-Firouzi et al., 2001). The silico module admetSAR has been used to characterize the various ADMET parameters for NiL (Cheng et al., 2012). ADMET analysis results are given in Table 5.

3.6. Docking studies

Molecular docking is an efficient calculation method in testing binding affinities of a molecule to a specific receptor. TSC show significant antitumor activity and their metal complexes are well known for their wide range of biological activities in most situations, although the underlying mechanism is not fully understood. As indicated in Krishnan et al. (2008) and Rao (2013), the antiproliferative activity of thiosemicarbazone can result from DNA binding and cleavage, activation of apoptosis, and inhibition of cell enzymes, and the planar thiosemicarbazone derivatives also display an intercalating function towards DNA and target DNA topoisomerase (Fu et al., 2017; Pelosi, 2010). Therefore, to expand our understanding of the effects of TSC metalcomplex, it is important to examine the mechanism involved in the change after its interaction with DNA. The three-dimensional crystal structure of DNA was obtained from the database of protein (PDB ID: 1BNA) (Drew et al., 1981). Hex (version 8.0.0) software (Ritchie, 2003; Ritchie & Kemp, 1999, 2000) was used for molecular docking with the following parameters: FFT mode—3D quick life, distance range—40, twist range—360, correlation type—shape + electro + DARS, grid dimension—0.6, receptor range—180, and ligand range—180. NiL molecule is bound to an active DNA site by hydrogen bonding interactions (Figure 7). The optimized structure of the NiL molecule calculated by DFT/B3LYP/6-311++G(d, p) is connected through intermolecular hydrogen bonds to DNA residues DT8, DC9, DG12, DG16, DA17 and DA18. Consequently, it follows that the docked ligand (NiL) formed a stable DNA complex.

The Interactions with nucleic acids are as follows:

- 4.95 Å long Pi–alkyl interaction between DT8 and Br atom;
- 4.55 Å long Pi–alkyl interaction between DC9 and Br atom;
- 3.35 Å long Halogen interaction between oxygen atom in DG12 and Br atom;
- 2.28 Å long unfavourable Bump; Halogen interaction between nitrogen atom in DG16 and Br atom;
- 4.55 Å long Pi–alkyl interaction between DG16 and Br atom;
- 3.43 Å long Pi–alkyl interaction between DA17 and Br atom;
- 3.92 Å long Pi–alkyl interaction between DA17 and Br atom;
- 4.79 Å long Pi–alkyl interaction between DA17 and Br atom;
- 5.46 Å long Pi–alkyl interaction between DA18 and NiL;
- 3.25 Å long Pi–alkyl interaction between DA18 and Br atom;
- 3.83 Å long Pi–alkyl interaction between DA18 and Br atom.

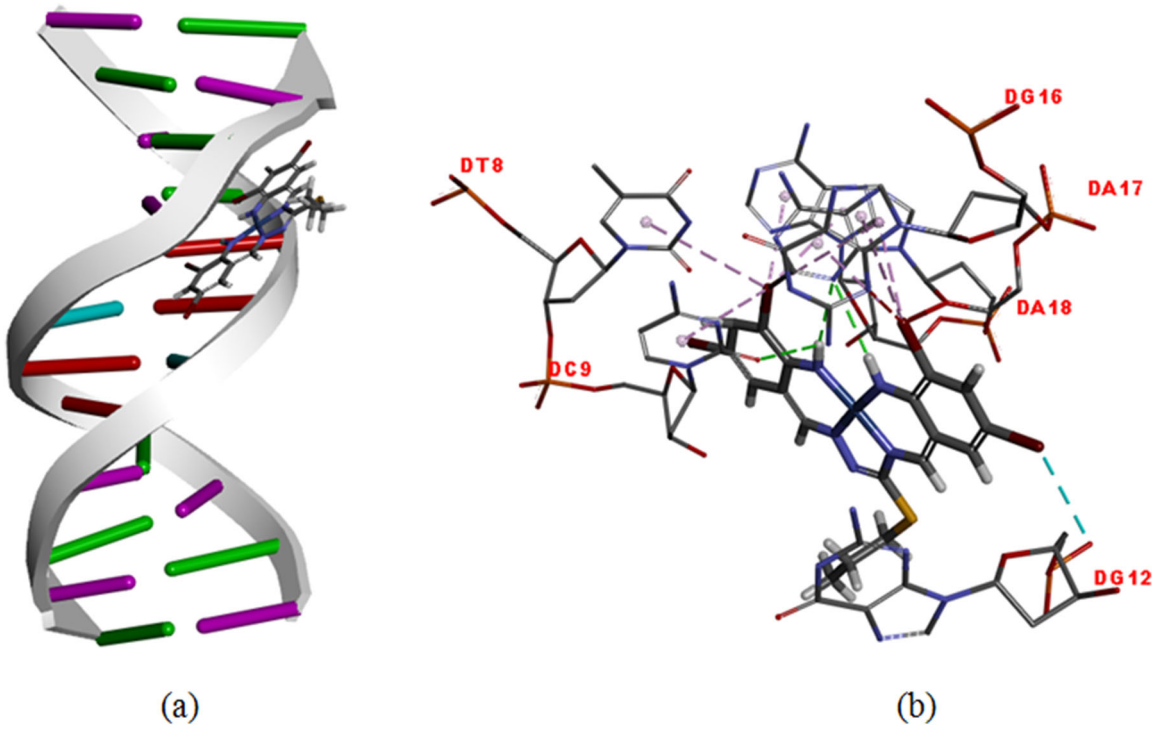

Figure 7. (a) Docking of NiL into DNA. (b) The detailed interactions of the optimized structure of NiL in gas phase.

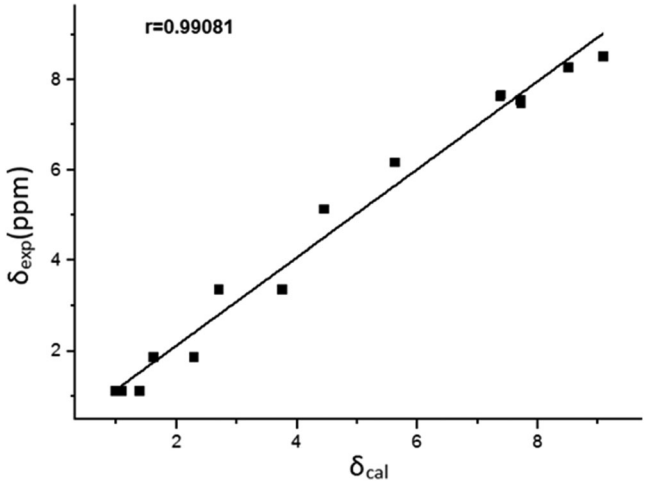

Figure 8. Plots of the experimental (δexp) and the theoretical chemical shifts (δcal) from the GIAO/B3LYP/6-311++G(d, p); NiL, proton.

Table 6. Chemical shifts (δ, ppm) for NiL in $CDCl_3$ and calculated GIAO nuclear magnetic shielding (σ_{cal}).

	δ_{exp}	δ_{cal}	σ_{cal}		δ_{exp}	δ_{cal}	σ_{cal}
C(1)		141.92	42.13	C(37)		16.00	168.05
C(2)		122.54	61.51	H(7)	7.67	7.38	24.59
C(3)		158.53	25.52	H(8)	7.55	7.71	24.27
C(4)		139.16	44.89	H(15)	7.64	7.37	24.60
C(5)		144.34	39.71	H(16)	7.49	7.72	24.25
C(6)		126.79	57.26	H(18)	5.14	4.44	27.53
C(9)		124.62	59.43	H(20)	6.18	5.62	26.35
C(10)		143.20	40.85	H(25)	8.52	9.08	22.89
C(11)		128.70	55.35	H(26)	8.28	8.50	23.47
C(12)		145.67	38.38	H(38)	3.37	3.75	28.22
C(13)		140.79	43.26	H(39)	3.37	2.69	29.28
C(14)		159.32	24.73	H(40)	1.87	1.61	30.36
C(21)		160.42	23.63	H(41)	1.87	2.28	29.70
C(23)		155.98	28.07	H(42)	1.12	1.38	30.59
C(32)		167.64	16.41	H(43)	1.12	1.09	30.89
C(35)		43.23	140.81	H(44)	1.12	0.97	31.01
C(36)		29.15	154.90				

3.7. NMR studies

The experimental ^{1}H-NMR spectra in $CDCl_3$ solution of the NiL is given as the supplementary file (Figure S3). The theoretical NMR spectrum of the title molecule is recreated by using B3LYP method and 6-311++G(d, p) as basis set. Chemical shifts were determined by subtracting the measured magnetic shielding value for the convenient nuclei from the reference molecule shielding value, tetramethylsilane (TMS) for 1H. The difference between the calculated values for protons and the correct values of experimental shifts is probably because of the calculation of shifts for single molecules in the gas phase. The correlation coefficient for proton was found to be 0.99081 and the correlation graphs are shown in Figure 8. The experimental and theoretical chemical shifts and the magnetic isotropic shielding values are also compared in Table 6. The distribution of the chemical shifts of protons related to the various functional groups, which are $-CH_2-CH_3$, $-CH_2-CH_2-CH_3$, $-O-CH_2-CH_3$, $-CH_2-CH_2-CH_2$, aromatic compounds, etc., owing to the variations in hydrogen bonding are easily recognizable in the NiL's ^{1}H-NMR spectrum and is given by the various splitting patterns.

4. Conclusions

Complex NiL was synthesized and characterized for the first time. The experimental and theoretical studies on the structure of NiL were carried out. The results obtained experimentally are in excellent agreement with those theoretically

calculated. The DFT/B3LYP/6-311++G(d, p) level of theory was used to calculate the optimized geometry, vibrational spectra and molecular electrostatic potential (MEP) map of the title compound. This study provides a theoretical basis for predicting the drug-likeness and absorption, distribution, metabolism, excretion and toxicity (ADMET) properties of NiL. The molecular docking studies indicated that the complex binds to DNA by H-bonding interactions and formed a stable DNA complex. By the study, the complex has been shown to have a potantial for drug ingredient agent targeting DNA.

Disclosure statement

No potential conflict of interest was reported by the authors.

Funding

This work was supported by the Scientific Research Projects Coordination Unit of Istanbul University [ÖNAP-2423], [23488].

References

Adams, M., de Kock, C., Smith, P. J., Chibale, K., & Smith, G. S. (2013). Synthesis, characterization and antiplasmodial evaluation of cyclopalladated thiosemicarbazone complexes. *Journal of Organometallic Chemistry*, *736*, 19–26. https://doi.org/10.1016/j.jorganchem.2013.02.024

Akinchan, N. T., Drożdżewski, P. M., & Holzer, W. (2002). Syntheses and spectroscopic studies on zinc (II) and mercury (II) complexes of isatin-3-thiosemicarbazone. *Journal of Molecular Structure*, *641*(1), 17–22. https://doi.org/10.1016/S0022-2860(02)00134-5

Amin, M. L. (2013). P-glycoprotein inhibition for optimal drug delivery. *Drug Target Insights*, *7*, 27–34. https://doi.org/10.4137/DTI.S12519

Bal-Demirci, T., Şahin, M., Özyürek, M., Kondakçı, E., & Ülküseven, B. (2014). Synthesis, antioxidant activities of the nickel (II), iron (III) and oxovanadium (IV) complexes with N2O2 chelating thiosemicarbazones. *Spectrochimica Acta Part A: Molecular and Biomolecular Spectroscopy*, *126*, 317–323. https://doi.org/10.1016/j.saa.2014.02.039

Bautista, J. L., Flores-Alamo, M., Tiburcio, J., Vieto, R., & Torrens, H. (2013). Synthesis and structural characterization of fluorinated thiosemicarbazones. *Molecules (Molecules)*, *18*(10), 13111–13123. https://doi.org/10.3390/molecules181013111

Becke, A. D. (1993). Density-functional thermochemistry. III. The role of exact exchange. *The Journal of Chemical Physics*, *98*(7), 5648–5652. https://doi.org/10.1063/1.464913

Behnisch, R., Mietzsch, F., & Schmidt, H. (1950). Chemical studies on thiosemicarbazones with particular reference to antituberculous activity. *American Review of Tuberculosis*, *61*(1), 1–7.

Bemis, G. W., & Murcko, M. A. (1999). Designing libraries with CNS activity. *Journal of Medicinal Chemistry*, *42*(24), 4942–4951. https://doi.org/10.1021/jm990017w

Bharanidharan, S., Saleem, H., Subashchandrabose, S., Suresh, M., & Ramesh Babu, N. (2017). FT-IR, FT-Raman and UV-Visible spectral analysis on (E)-N′-(thiophen-2-ylmethylene) nicotinohydrazide. *Archives in Chemical Research*, *1*, 2.

Bisceglie, F., Bacci, C., Vismarra, A., Barilli, E., Pioli, M., Orsoni, N., & Pelosi, G. (2020). Antibacterial activity of metal complexes based on cinnamaldehyde thiosemicarbazone analogues. *Journal of Inorganic Biochemistry*, *203*, 110888. https://doi.org/10.1016/j.jinorgbio.2019.110888

Casas, J. S., García-Tasende, M. S., & Sordo, J. (2000). Main group metal complexes of semicarbazones and thiosemicarbazones. A structural review. *Coordination Chemistry Reviews*, *209*(1), 197–261. https://doi.org/10.1016/S0010-8545(00)00363-5

Celik, S., Akyuz, S., & Ozel, A. E. (2017). Vibrational spectroscopic and structural investigations of bioactive molecule Glycyl-Tyrosine (Gly-Tyr). *Vibrational Spectroscopy*, *92*, 287–297. https://doi.org/10.1016/j.vibspec.2017.08.007

Celik, S., Albayrak, A. T., Akyuz, S., E., & Ozel, A. (2019). Molecular modelling and vibrational investigations of ammonium-based ionic liquid (CLTOAB). *Journal of Biomolecular Structure & Dynamics*, *37*(10), 2515–2526. https://doi.org/10.1080/07391102.2018.1495578

Cheng, F., Li, W., Zhou, Y., Shen, J., Wu, Z., Liu, G., Lee, P. W., & Tang, Y. (2012). admetSAR: A comprehensive source and free tool for evaluating chemical ADMET properties. *Journal of Chemical Information and Modeling*, *52*(11), 3099–3105. https://doi.org/10.1021/ci300367a

Das, S., Bharanidharan, S., & Dhandapani, A. (2018). Molecular spectroscopy and molecular docking studies on (E)-1-(4-bromobenzylidene) thiourea. *Journal of New Developments in Chemistry*, *1*(3), 62–81. https://doi.org/10.14302/issn.2377-2549.jndc-18-1933

Drew, H. R., Wing, R. M., Takano, T., Broka, C., Tanaka, S., Itakura, K., & Dickerson, R. E. (1981). Structure of a B-DNA dodecamer: Conformation and dynamics. *Proceedings of the National Academy of Sciences of the United States of America*, *78*(4), 2179–2183. https://doi.org/10.1073/pnas.78.4.2179

Eglence-Bakir, S., Sacan, O., Sahin, M., Yanardag, R., & Ulkuseven, B. (2019). Dioxomolybdenum (VI) complexes with 3-methoxy salicylidene-N-alkyl substituted thiosemicarbazones. Synthesis, characterization, enzyme inhibition and antioxidant activity. *Journal of Molecular Structure*, *1194*, 35–41.

Ertl, P., Rohde, B., & Selzer, P. (2000). Fast calculation of molecular polar surface area as a sum of fragment-based contributions and its application to the prediction of drug transport properties. *Journal of Medicinal Chemistry*, *43*(20), 3714–3717. https://doi.org/10.1021/jm000942e

Finch, A., & Pillans, P. (2014). P-glycoprotein and its role in drug-drug interactions. *Australian Prescriber*, *37*(4), 137–139. https://doi.org/10.18773/austprescr.2014.050

Frisch, M. J., Trucks, G. W., Schlegel, H. B., Scuseria, G. E., Robb, M. A., Cheeseman, J. R., … Pople, J. A. (2004). *Gaussian 03, revision C. 02*. Gaussian, Inc.

Fu, Y., Liu, Y., Wang, J., Li, C., Zhou, S., Yang, Y., Zhou, P., Lu, C., & Li, C. (2017). Calcium release induced by 2-pyridinecarboxaldehyde thiosemicarbazone and its copper complex contributes to tumor cell death. *Oncology Reports*, *37*(3), 1662–1670. https://doi.org/10.3892/or.2017.5395

Ghogomu, J. N., & Nkungli, N. K. (2016). A DFT study of some structural and spectral properties of 4-methoxyacetophenone thiosemicarbazone and its complexes with some transition metal chlorides: Potent antimicrobial agents. *Advances in Chemistry*, *2016*, 1–15. https://doi.org/10.1155/2016/9683630

Griffiths, P. R., Thompson, H. W. (1967). Far infrared spectra and vibrational assignments of substituted benzenes. *Proceedings of the Royal Society of London. Series A. Mathematical and Physical Sciences*, *298*, 51–63. https://doi.org/ https://doi.org/10.1098/rspa.1967.0089

Güveli, Ş., Agopcan Çınar, S., Karahan, Ö., Aviyente, V., & Ülküseven, B. (2016). Nickel (II)–PPh_3 complexes of S, N-substituted thiosemicarbazones–structure, DFT study, and catalytic efficiency. *European Journal of Inorganic Chemistry*, *2016*(4), 538–544. https://doi.org/10.1002/ejic.201501227

Istvan, K. (2002). *Simirra, A program for simulation of IR and Raman spectra*. Budapest: Chemical Research Center (It was obtained from Dr. Gabor Keresztury in Chemical Research Center in Budapest).

Krishnan, K., Prathiba, K., Jayaprakash, V., Basu, A., Mishra, N., Zhou, B., Hu, S., & Yen, Y. (2008). Synthesis and ribonucleotide reductase inhibitory activity of thiosemicarbazones. *Bioorganic & Medicinal Chemistry Letters*, *18*(23), 6248–6250. https://doi.org/10.1016/j.bmcl.2008.09.097

Kurt, Y., Ilhan-Ceylan, B., Açıkgöz, M., Tüzün, E., Atun, G., & Ülküseven, B. (2013). N_2O_2-complexes of oxovanadium (IV) with 2, 2′-dihydroxybenzophenone thiosemicarbazones: Synthesis, EPR and electrochemical studies. *Polyhedron*, *65*, 67–72. https://doi.org/10.1016/j.poly.2013.08.010

Lea, T. (2015). Caco-2 cell line. In Verhoeckx K, Cotter P, Lopez-Exposito I. (Eds.) *The impact of food bioactives on health: In vitro and ex vivo models.* Springer.

Leovac, V. M., Gerbeleu, N. V., & Canic, V. D. (1982). Coordination compounds of cobalt (III), chromium (III), and vanadium (III) with salicylaldehyde S-methylthiosemicarbazone. *Russian* Journal of Inorganic Chemistry., *27*, 514–517.

Matsa, R., Makam, P., Kaushik, M., Hoti, S. L., & Kannan, T. (2019). Thiosemicarbazone derivatives: Design, synthesis and in vitro antimalarial activity studies. *European Journal of Pharmaceutical Sciences*, *137*, 104986. https://doi.org/10.1016/j.ejps.2019.104986

Mishra, D., Naskar, S., Drew, M. G., & Chattopadhyay, S. K. (2006). Synthesis, spectroscopic and redox properties of some ruthenium (II) thiosemicarbazone complexes: Structural description of four of these complexes. *Inorganica Chimica Acta*, *359*(2), 585–592. https://doi.org/10.1016/j.ica.2005.11.001

Molinspiration Cheminformatics. (n.d.). Retrieved from: http://www.molinspiration.com

Nehar, O. K., Mahboub, R., Louhibi, S., Roisnel, T., & Aissaoui, M. (2020). New thiosemicarbazone Schiff base ligands: Synthesis, characterization, catecholase study and hemolytic activity. *Journal of Molecular Structure*, *1204*, 127566. https://doi.org/10.1016/j.molstruc.2019.127566

Netalkar, P. P., Netalkar, S. P., & Revankar, V. K. (2014). Nickel (II) complexes of thiosemicarbazones: Synthesis, characterization, X-ray crystallographic studies and in vitro antitubercular and antimicrobial studies. *Transition Metal Chemistry*, *39*(5), 519–526. https://doi.org/10.1007/s11243-014-9827-8

Netalkar, P. P., Netalkar, S. P., & Revankar, V. K. (2015). Transition metal complexes of thiosemicarbazone: Synthesis, structures and in vitro antimicrobial studies. *Polyhedron*, *100*, 215–222.

OSIRIS Property Explorer (2010). Allschwil, Switzerland: Actelion Pharmaceuticals Ltd.. Retreived from: http://www.organic-chemistry.org/prog/peo/

Padhye, S., & Kauffman, G. B. (1985). Transition metal complexes of semicarbazones and thiosemicarbazones. *Coordination Chemistry Reviews*, *63*, 127–160. https://doi.org/10.1016/0010-8545(85)80022-9

Patra, D., Paul, S., Sepay, N., Kundu, R., & Ghosh, T. (2018). Structure–activity relationship on DNA binding and anticancer activities of a family of mixed-ligand oxidovanadium(V) hydrazone complexes. *Journal of Biomolecular Structure & Dynamics*, *36*(16), 4143–4155. https://doi.org/10.1080/07391102.2017.1409652

Pearson, R. G. (1973). *Hard and soft acids and bases.* (Vol.2). Van Nostrand Reinhold.

Pelosi, G. (2010). Thiosemicarbazone metal complexes: From structure to activity. *The Open Crystallography Journal*, *3*(2), 16–28. https://doi.org/10.2174/1874846501003020016

Piippo, K., Laitinen, P., Swan, H., Toivonen, L., Viitasalo, M., Pasternack, M., Paavonen, K., Chapman, H., Wann, K. T., Hirvela, E., Sajantila, A., & Kontula, K. (2000). Homozygosity for a HERG potassium channel mutation causes a severe form of long QT syndrome: Identification of an apparent founder mutation in the Finns. *Journal of the American College of Cardiology*, *35*(7), 1919–1925. https://doi.org/10.1016/S0735-1097(00)00636-7

Pulay, P., Fogarasi, G., Pongor, G., Boggs, J. E., & Vargha, A. (1983). Combination of theoretical ab initio and experimental information to obtain reliable harmonic force constants. Scaled quantum mechanical (QM) force fields for glyoxal, acrolein, butadiene, formaldehyde, and ethylene. *Journal of the American Chemical Society*, *105*(24), 7037–7047. https://doi.org/10.1021/ja00362a005

Rao, V. A. (2013). Iron chelators with topoisomerase-inhibitory activity and their anticancer applications. *Antioxidants & Redox Signaling*, *18*(8), 930–955. https://doi.org/10.1089/ars.2012.4877

Ritchie, D. W. (2003). Evaluation of protein docking predictions using Hex 3.1 in CAPRI rounds 1 and 2. *Proteins: Structure, Function, and Genetics*, *52*(1), 98–106. https://doi.org/10.1002/prot.10379

Ritchie, D. W., & Kemp, G. J. (1999). Fast computation, rotation, and comparison of low resolution spherical harmonic molecular surfaces. *Journal of Computational Chemistry*, *20*(4), 383–395. https://doi.org/10.1002/(SICI)1096-987X(199903)20:4<383::AID-JCC1>3.0.CO;2-M

Ritchie, D. W., & Kemp, G. J. (2000). Protein docking using spherical polar Fourier correlations. *Proteins: Structure, Function, and Genetics*, *39*(2), 178–194. https://doi.org/10.1002/(SICI)1097-0134(20000501)39:2<178::AID-PROT8>3.0.CO;2-6

Sadler, P. W. (1961). Synthesis of antiviral agents. Part I. Heterocyclic compounds related to isatin 3-thiosemicarbazone. *Journal of the Chemical Society (Resumed))*, *1961*, 243–246. https://doi.org/10.1039/jr9610000243

Şahin, M., Eğlence-Bakır, S., Alpay, M., Alpay, S., Özmerdivenli, R., & Ülküseven, B. (2020). Effective copper (II) and nickel (II) complexes with N_3O and ON_3 thiosemicarbazidato ligands. Synthesis, structural analysis and in vitro cytotoxity on melanoma B16F10 cells. *Inorganica Chimica Acta*, *502*, 119347. https://doi.org/10.1016/j.ica.2019.119347

Sankaraperumal, A., Karthikeyan, J., Shetty, A. N., & Lakshmisundaram, R. (2013). Nickel (II) complex of p-[N, N-bis (2-chloroethyl) amino] benzaldehyde-4-methyl thiosemicarbazone: Synthesis, structural characterization and biological application. *Polyhedron*, *50*(1), 264–269. https://doi.org/10.1016/j.poly.2012.11.006

Sert, Y., Miroslaw, B., Çırak, Ç., Doğan, H., Szulczyk, D., & Struga, M. (2014). Vibrational spectroscopy (FT-IR and Laser-Raman) investigation, and computational (M06-2X and B3LYP) analysis on the structure of 4-(3-fluorophenyl)-1-(propan-2-ylidene)-thiosemicarbazone. *Spectrochimica Acta Part A: Molecular and Biomolecular Spectroscopy*, *128*, 91–99. https://doi.org/10.1016/j.saa.2014.02.134

Sens, L., Oliveira, A. S. D., Mascarello, A., Brighente, I., Yunes, R. A., & Nunes, R. J. (2018). Synthesis, Antioxidant activity, acetylcholinesterase inhibition and quantum studies of thiosemicarbazones. *Journal of the Brazilian Chemical Society*, *29*(2), 343–352.

Shao, Y., Molnar, L. F., Jung, Y., Kussmann, J., Ochsenfeld, C., Brown, S. T., Gilbert, A. T. B., Slipchenko, L. V., Levchenko, S. V., O'Neill, D. P., DiStasio Jr, R. A., Lochan, R. C., Wang, T., Beran, G. J. O., Besley, N. A., Herbert, J. M., Yeh Lin, C., Van Voorhis, T., Hung Chien, S., … Head-Gordon, M. (2006). Advances in methods and algorithms in a modern quantum chemistry program package. *Physical Chemistry Chemical Physics*, *8*(27), 3172–3191. https://doi.org/10.1039/B517914A

Shawish, M., & Bashir, H. (2014). *Synthesis, characterization and biological studies of nickel (II) complexes containing thiosemicarbazone and thiourea derivatives/Hana Bashir Mohammed Shawish* [Doctoral dissertation], University of Malaya.

Sheweita, S. A. (2000). Drug-metabolizing enzymes mechanisms and functions. *Current Drug Metabolism*, *1*(2), 107–132. https://doi.org/10.2174/1389200003339117

Singh, R. K., & Singh, A. K. (2015). Synthesis, molecular structure, spectral analysis, natural bond order and intramolecular interactions of 2-acetylpyridine thiosemicarbazone: A combined DFT and AIM approach. *Journal of Molecular Structure*, *1094*, 61–72. https://doi.org/10.1016/j.molstruc.2015.03.064

Singh, S. I., & Shamir, J. (1977). Polarised Raman and infrared spectra of single crystals of P-chlorobromobenzene. *Indian Journal of Physics*, *51*, 50–57.

Sundius, T. (1990). Molvib – A flexible program for force field calculations. *Journal of Molecular Structure*, *218*, 321–326. https://doi.org/10.1016/0022- 2860(90)80287-Thttps://doi.org/10.1016/0022-2860(90)80287-T

Sundius, T. (2002). Scaling of ab initio force fields by MOLVIB. *Vibrational Spectroscopy*, *29*(1-2), 89–95. https://doi.org/10.1016/S0924-2031(01)00189-8

Suzuki, M. (1977). Vibrational spectra of bexabromobenzene and hexaiodobenzene. *Spectrochimica Acta Part A: Molecular Spectroscopy*, *33*(10), 921–927. https://doi.org/10.1016/0584-8539(77)80092-5

Tristani-Firouzi, M., Chen, J., Mitcheson, J. S., & Sanguinetti, M. C. (2001). Molecular biology of K+channels and their role in cardiac arrhythmias. *The American Journal of Medicine*, *110*(1), 50–59. https://doi.org/10.1016/S0002-9343(00)00623-9

Varsanyi, G. (1974). *Assignments for vibrational spectra of seven hundred benzene derivatives* (Vol.1). Halsted Press.

Varsanyi, G. (2012). *Vibrational spectra of benzene derivatives*. Elsevier.

Yamashita, S., Furubayashi, T., Kataoka, M., Sakane, T., Sezaki, H., & Tokuda, H. (2000). Optimized conditions for prediction of intestinal drug permeability using Caco-2 cells. *European Journal of*

Pharmaceutical Sciences, *10*(3), 195–204. https://doi.org/10.1016/S0928-0987(00)00076-2

Yee, S. (1997). In vitro permeability across Caco-2 cells (colonic) can predict in vivo (small intestinal) absorption in man—fact or myth. *Pharmaceutical Research*, *14*(6), 763–766. https://doi.org/10.1023/A:1012102522787

Zanger, U. M., & Schwab, M. (2013). Cytochrome P450 enzymes in drug metabolism: Regulation of gene expression, enzyme activities, and impact of genetic variation. *Pharmacology & Therapeutics*, *138*(1), 103–141. https://doi.org/10.1016/j.pharmthera.2012.12.007

Zhao, Y. H., Le, J., Abraham, M. H., Hersey, A., Eddershaw, P. J., Luscombe, C. N., Butina, D., Beck, G., Sherborne, B., Cooper, I., Platts, J. A., & Boutina, D. (2001). Evaluation of human intestinal absorption data and subsequent derivation of a quantitative structure–activity relationship (QSAR) with the Abraham descriptors. *Journal of Pharmaceutical Sciences*, *90*(6), 749–784. https://doi.org/10.1002/jps.1031